Photonic band gaps in optical lattices

I. H. Deutsch, R. J. C. Spreeuw,* S. L. Rolston, and W. D. Phillips
National Institute of Standards and Technology, PHYS A167, Gaithersburg, Maryland 20899
(Received 31 August 1994; revised manuscript received 5 December 1994)

We study photonic band gaps in a one-dimensional optical lattice of laser-cooled trapped atoms. We solve for the self-consistent equilibrium positions of the atoms, accounting for the backaction of the atoms on the trapping beams. This solution depends strongly on the sign of the trapping laser detuning. For red-detuned trapping lasers, the resulting lattice exhibits a one-dimensional photonic band gap for frequencies between the trapping laser frequency and the atomic resonance. For blue detuning the stop band extends symmetrically about resonance, typically for hundreds of atomic linewidths, except for the small region between atomic resonance and the lattice frequency, which is excluded. We calculate the reflection spectrum for a lattice of Cs atoms for various trapping laser detunings and interpret its behavior as a function of the lattice size and density. For a mean density of 10^{11} cm^{-3}, and 1000 planes, 55% reflection of a weak probe beam should be observed. We also consider Bragg scattering in a three-dimensional optical lattice as a means of probing the long-range order in the atomic density correlation function.

PACS number(s): 32.80.Pj, 42.50.Gy

I. INTRODUCTION

Laser-cooled atoms can be trapped at periodic spatial positions in one [1,2], two, or three [3–6] dimensions by ac Stark shift potential wells created by the interference of multiple laser beams. These "optical lattices" constitute a form of matter in which atoms are located at periodic sites separated on the scale of the optical wavelength. At currently achieved densities, atoms occupy very few of the available sites. Even so, the strict periodicity in the trapping positions should give rise to correlations in the atomic positions over very long distances.

This long-range spatial order will have dramatic consequences for the propagation of light. In a disordered gas the interference between incident and forward-scattered waves is described simply by a macroscopic complex index of refraction. Such a description is no longer valid when the positions of the atoms are periodically ordered. The scattered waves are now spatially correlated so that the coherence length for interference in directions other than the forward direction will be large. Situations may occur that are analogous to Bragg scattering of x rays by solid-state crystals. When a probe beam propagates normal to a set of planes separated by a $\lambda/2$, interference between forward and backward waves can strongly attenuate the incident field and enhance the reflected wave. For sufficient densities multiple scattering becomes important, as in the "dynamic" Bragg scattering of x rays in crystals, and strong reflection is expected for a wide range of probe frequencies. This "photonic band gap" in one dimension is analogous to strong reflection obtained from multilayer thin-film dielectric mirrors [7].

There is currently active research to develop materials possessing three-dimensional photonic band gaps that suppress propagation of light of a given frequency range in all directions [8]. The key to producing such a band gap is to engineer a periodic dielectric material with strong Bragg scattering in all directions. The frequency and direction of these scattering resonances are described by the surface of the first Brillouin zone (BZ) in the reciprocal-lattice space of the periodic structure. The bandwidth of the three-dimensional band gap is given by the overlap of all the one-dimensional gaps associated with each point on the BZ surface over 4π sr. In contrast to solid dielectric media, the scattering strength of an optical lattice is very weak, except near atomic resonance. Thus the only points on the BZ surface with a non-negligible band gap are those whose frequency is almost equal to the atomic resonance frequency. In addition, the atomic polarizability is highly polarization dependent, further reducing the surface of the BZ covered by strong band gaps. Therefore, an optical lattice will not generally contain higher-dimensional photonic band gaps, even if it is densely occupied and very large. Our considerations are thus restricted solely to the observation of a one-dimensional gap.

An intriguing aspect of the optical lattice is the propagation of the very light that creates it. For atoms trapped at the nodes or antinodes of a standing wave, the periodicity appears to be just right for Bragg scattering of the trapping lasers. In other words, the light seems to create a structure into which it cannot propagate. This paradox leads us to a self-consistent analysis of the trapping of cold atoms in an off-resonance standing wave. Having done this, we then turn to study how a weak probe propagates in the self-consistent lattice.

The general structure of our analysis is as follows. First we consider the interaction of the atoms with the laser beams that define the optical lattice, in order to determine the equilibrium atomic positions. This is accomplished in Sec. II, where we treat the entire system in

*Present address: University of Konstanz, Fakultät für Physik, Postfach 5560 M696, D-78434 Konstanz, Germany.

a self-consistent manner, including the effect of the atomic response on the propagation of these beams. The presence of the atoms modifies the distribution of field energy, which in turn modifies the equilibrium position of the atoms. For trapping lasers detuned to the red of atomic resonance, we find that the self-consistent lattice has a period slightly less than $\lambda/2$; for blue detuning the period is exactly $\lambda/2$.

Having determined the equilibrium positions of the atoms in the lattice, we turn to study the propagation of a weak probe in this medium (one may imagine that the trapping lasers that define the lattice are turned off during the probing phase, which is performed rapidly enough that the atoms do not significantly move from their initial positions). In Sec. III we calculate the photonic band gap associated with an infinite lattice and the reflection and transmission coefficients of the probe incident on a finite lattice. For an arbitrary trapping lattice (either red or blue), the trapping laser frequency is on a band edge so that it can penetrate the structure infinitely far. The dependence of the reflection coefficient on the frequency of the probe is governed by two effects: phase shifts accumulated as the scattered waves propagate between atomic planes and dispersion in the local atomic response. In contrast to multilayered dielectric thin films, the latter effect in the optical lattice plays a dominant role in the mode dispersion. We will see that the effects of both local dispersion and global interference will dramatically alter the behavior of the probe reflection curve as a function of frequency when the length or density of the lattice is increased.

In Sec. IV we study the feasibility of observing these effects in the laboratory concentrating mainly on a one-dimensional lattice, i.e., thin slabs of atoms localized at periodic positions, trapped by counterpropagating orthogonally polarized lasers. For a lattice of cesium atoms with a density of 10^{11} atoms/cm^3, a total of 1000 planes, and lattice laser beams detuned 10 natural linewidths below resonance, the peak reflection for a circularly polarized probe at the atomic resonance is 55%.

In Sec. V we will briefly explore Bragg scattering in a three-dimensional lattice. Since the atoms remain at their periodic locations for some time after the trapping lasers are turned off, one can perform a transient experiment to observe the decay of the reflected field as the atomic positions become random, giving unambiguous proof of the long-range spatial order of the lattice. Previous spectroscopic experiments of probe propagation in these structures have exhibited probe reflection [4,9]. Because the lattice and probe lasers were present simultaneously, this observation can equally well be interpreted as a nonlinear four-wave mixing between the lattice laser beams and the weak probe in a uniform gas of atoms. By performing a transient experiment in the absence of the "pump" laser, four-wave mixing is eliminated as a possible mechanism. However, the lattice lasers may imprint a "spin grating" on a uniform gas due to optical pumping associated with the local electric-field polarization, which would also Bragg scatter a probe beam [10]. We examine how a particular choice of three-dimensional laser geometry might provide an unambiguous demonstration of long-range modulation of the total atomic density. In Sec. VI we will interpret the predicted effects in terms of the fundamental processes of spontaneous and stimulated photon emission and summarize our results.

II. SELF-CONSISTENT OPTICAL LATTICE

Here we consider a one-dimensional optical lattice formed when ultracold atoms are trapped in periodic potential wells created by the ac Stark shift associated with a uniformly polarized standing electromagnetic wave. For simplicity, in the discussion to follow we will assume that the atoms are maintained at sufficiently cold temperatures by an unspecified mechanism and remain trapped for long times. When studying the propagation of light in this lattice, the following apparent paradox arises. The distance between optical potential wells of the standing wave that trap the atoms is $\lambda/2$, the spacing at which light of that frequency would Bragg scatter into the backward direction. If the density were sufficiently high, it would appear that the trapping laser could not propagate into the ordered collection of atoms bound at these sites. The resolution of this paradox lies in the important backaction of the atoms on the light. The propagation of the light is modified by interference between incident and scattered waves. This scattering will redistribute the field energy, thereby changing the light forces on the atoms. We therefore seek a self-consistent equilibrium solution for the entire atom-field system.

Consider first the scattering of a plane wave by atoms randomly arranged in a plane. For low intensities, all scattered radiation (resonance fluorescence) is coherent. We can thus calculate the reflection and the transmission coefficients by considering the classical scattering of a wave from a plane of polarizable particles, with surface density η particles per unit area and polarizability α per particle. In general, the randomly distributed discrete atoms will give rise to Rayleigh scattering losses due to the density fluctuations of atoms in the plane. As long as the distance between atoms is large compared to the optical wavelength and many atoms are contained within the coherence area of the beam, the calculation of the fields scattered solely into the forward and the backward directions is well modeled by a continuous homogeneous sheet of equal average density, but with an imaginary part ascribed to its polarizability [11]. For the discussion to follow we will be considering atoms excited far from resonance where the imaginary part is small and thus scattering losses are negligible. We will return to the complete expression in Sec. III.

The one-dimensional wave equation for a monochromatic wave $E(z)e^{-i\omega t}$ propagating at normal incidence to a polarizable plane at $z=0$ is

$$[\partial_z^2+k^2]\mathbf{E}=-4\pi k^2\mathbf{P}=-4\pi k^2\eta\alpha\delta(z)\mathbf{E}\ , \tag{1}$$

where $k=\omega/c$. The electric field tangential to the plane is continuous and the δ function localization of the polarization $\mathbf{P}$ leads to a discontinuity in the derivative of the electric field (and the value of the magnetic field). Integrating Eq. (1) on a small interval centered at $z=0$

leads to the boundary conditions

$$\mathbf{E}(z=0_+)=\mathbf{E}(z=0_-)\ , \tag{2a}$$

$$\partial_z\mathbf{E}(z=0_-)-\partial_z\mathbf{E}(z=0_+)=4\pi k^2\eta\alpha\mathbf{E}(z=0)\ . \tag{2b}$$

Considering a field propagating in the positive z direction $\mathbf{E}_{\rm inc}=\mathbf{E}_0e^{ikz}$ and reflected and transmitted fields $\mathbf{E}_{\rm ref}=r\mathbf{E}_0e^{-ikz}$ and $\mathbf{E}_{\rm trans}=t\mathbf{E}_0e^{ikz}$, the boundary conditions give

$$r=\frac{i\zeta}{1-i\zeta},\quad t=\frac{1}{1-i\zeta}\ , \tag{3a}$$

where

$$\zeta=2\pi k\eta\alpha\ . \tag{3b}$$

Note that for α real, the energy in the forward- and the backward-going modes is conserved, and is characterized by the conditions $|r|^2+|t|^2=1$ and $rt^*+r^*t=0$. In that case, the reflection and the transmission coefficients can be written as $r=i\sin\phi e^{i\phi}$ and $t=\cos\phi e^{i\phi}$, where

$$\phi=\tan^{-1}(\zeta) \tag{4}$$

is the phase shift upon transmission.

Now we can determine the equilibrium position of a plane of atoms in a standing wave. Consider an atomic plane placed at $z=z_0$ with a traveling wave E_0e^{-ikz} incident from the right and E_0e^{ikz} from the left. The total fields, including those scattered by the atoms, on the left- and the right-hand sides of the plane are

$$\mathbf{E}_L=\mathbf{E}_0e^{ikz}+r\mathbf{E}_0e^{-ik(z-2z_0)}+t\mathbf{E}_0e^{-ikz},\quad z\le z_0 \tag{5a}$$

$$\mathbf{E}_R=\mathbf{E}_0e^{-ikz}+r\mathbf{E}_0e^{ik(z-2z_0)}+t\mathbf{E}_0e^{ikz},\quad z\ge z_0\ , \tag{5b}$$

respectively. The local intensity at the plane is thus

$$|\mathbf{E}_L(z=z_0)|^2=|\mathbf{E}_R(z=z_0)|^2=4|t|^2|\mathbf{E}_0|^2\cos^2kz_0\ , \tag{6}$$

where we have used the relation $t=1+r$ as follows from Eq. (3a).

If the optical lattice is created with lasers detuned to the red of the atomic resonance, the atoms are attracted to regions of high intensity. The atomic equilibrium positions correspond to a maximum of the local intensity, which by Eq. (6) corresponds to $kz_0=0$, so that Eqs. (5) become

$$\mathbf{E}_L=\mathbf{E}_0e^{ikz}+(r+t)\mathbf{E}_0e^{-ikz}=2\mathbf{E}_0\cos(kz-\phi)e^{i\phi}\ ,\quad z\le 0 \tag{7a}$$

$$\mathbf{E}_R=\mathbf{E}_0e^{-ikz}+(r+t)\mathbf{E}_0e^{ikz}=2\mathbf{E}_0\cos(kz+\phi)e^{i\phi}\ ,\quad z\ge 0\ , \tag{7b}$$

respectively, where we have assumed that the polarizability is real. This field is a standing wave with a "phase slip" 2ϕ at the atomic plane. For red detuning ϕ is positive, so that the atoms seem to "pull" the nodes closer to the plane. Repeating this procedure at every antinode results in a phase slip at every plane and a slight change in the spatial periodicity of the standing wave (Fig. 1). Since this configuration is self-consistent, with zero net force on the atoms, it must represent a state of minimum potential energy.

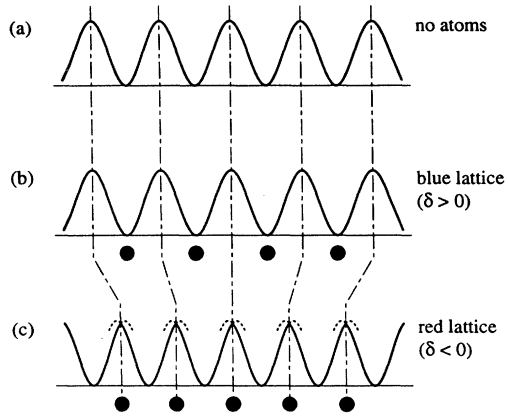

FIG. 1. The self-consistent lattice arises from a redistribution of photons in a standing wave due to phase shifts induced by periodically trapped atoms. (a) shows the standing wave in the absence of atoms. For a standing wave detuned to the blue of the atomic resonance shown in (b), atoms are trapped at the nodes and thus the period of the standing wave is equal to its vacuum value. A standing wave detuned to the red of resonance traps atoms at the antinodes, which leads phase shifts of the field. The solution shown in (c) is such that the nodes are "pulled" closer to the atomic planes and the resulting standing wave has a reduced effective wavelength with cusps at its antinodes [Eq. (2b)].

For an optical lattice created with lasers detuned to the blue, the situation is markedly different. In this case the equilibrium position corresponds to minimum intensity, or $kz_0=\pi/2$. Substituting this into Eq. (6), we see that the self-consistent field is simply a standing wave as if no atoms were present:

$$\mathbf{E}_L=\mathbf{E}_R=\mathbf{E}_0(e^{ikz}+e^{-ikz})=2\mathbf{E}_0\cos(kz)\ . \tag{8}$$

Thus an equilibrium configuration for the total atom-field system for blue detuning results when a plane of atoms is placed at the node of a standing wave (Fig. 1) [12].

The self-consistent equilibrium solution gives the period between planes d,

$$k_Ld=\pi-\xi\phi_L\rightarrow d=\frac{\lambda_L}{2}\left[1-\frac{\xi\phi_L}{\pi}\right]\ ,\quad \xi\equiv 1-\mathrm{sgn}(\delta_L)\ , \tag{9}$$

where k_L and ϕ_L are the wave vector and the phase shift at the lattice laser frequency and δ_L is the detuning from atomic resonance. The phase shift ϕ_L depends on the atomic density and thus, for red detuning, the lattice constant d will have such a dependence, whereas for blue detuning it is independent of density. According to this self-consistent solution, the effective wavelength of the light inside the medium is $\lambda_{\rm eff}=\lambda_L(1-\xi\phi/\pi)$. A change in the wavelength of the light propagating in an atomic gas is not unexpected, given an effective index of refrac-

tion. For a disordered gas with bulk density $N=\eta/d\approx\eta k/\pi$, the index of refraction is $n_{\rm ref}\approx 1+2\pi N\alpha=1+\phi/\pi$ and the wavelength inside the gas is $\lambda_{\rm eff}=\lambda/n_{\rm ref}=\lambda(1-\phi/\pi)$. The factor of $\xi\neq 1$ in the phase shift arises from coherent interference of the backward-scattered waves, possible only for the spatially ordered lattice. For red detuning, atoms at the antinodes give rise to equal phase shifts for forward- and backward-scattered waves, while for blue detuning these phase shifts are equal, but of opposite sign so that $\xi=0$. Alternatively, we may view the equality between the standing-wave wavelength in the blue-detuned lattice and in vacuum from the fact that the atoms are trapped at the nodes and thus do not influence the propagation lattice light. Note that the sole effect of the detuning of the trapping laser beam is to determine the periodicity of the planar positions. In the next section we will see how this parameter is crucial in determining the boundaries of the photonic band gap experienced by a weak beam that probes the lattice. In particular, we will see that the self-consistent lattice resolves the paradox stated at the beginning of this section: the trapping beams lie at the edge of the photonic band gap and thus propagate into the structure as an unattenuated standing wave.

III. ONE-DIMENSIONAL BAND GAP

The propagation of light in an infinite one-dimensional lattice of atoms perfectly localized in planes is formally equivalent to the Kronig-Penney model of electron de Broglie waves in a one-dimensional lattice of δ-function potentials. The resulting modes satisfy Bloch's theorem, with a gap in the allowed energies at the Brillouin zone edges. Exactly at the band edge, the group velocity of the Bloch wave approaches zero, corresponding to the condition for Bragg scattering. The resulting wave function is a standing wave, with antinodes (nodes) at the scattering centers at the low-frequency band edge for attractive (repulsive) potentials and nodes (antinodes) at the high-frequency edge. For the case of the optical lattice, we found that trapping laser beams are arranged in standing waves such that the total system has a minimum potential energy. These observations suggest that the self-consistent assembly of atomic planes will have a photonic band gap with a low-frequency edge corresponding to the frequency of the laser used to define the lattice.

Formally speaking, the above discussion applies solely to the case of an infinite lattice, where Bloch's theorem is strictly true. For the case of a finite lattice, band gaps manifest themselves as "tunneling barriers," whereby the transmitted field is exponentially damped for frequencies inside the gap. For a truly one-dimensional lossless structure, all nontransmitted energy is reflected. Clearly, in order to observe substantial reflection over the entire stop band, the length of the lattice must be longer than the excitation length associated with this tunneling barrier. Furthermore, competing with the attenuation due to coherent interference is attenuation due to absorption. Thus, even in the infinite lattice limit we do not expect a perfect stop band. We seek a complete expression for the band-gap dispersion relation and the transmission and

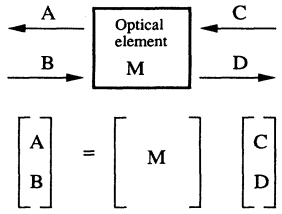

FIG. 2. The transfer-matrix method relates forward- and backward-traveling waves on the right-hand side of an arbitrary linear optical element to those on the left-hand side. This allows for a simple method to calculate the propagation through a series of elements, automatically accounting for multiple reflections and all interference effects. A,B,C, and D are the amplitudes of the fields.

the reflection coefficients of a finite structure seen by a weak probe for a lattice composed of periodically spaced atomic planes. These can be calculated easily by the transfer-matrix method [13], which relates forward- and backward-going waves on the right-hand side of any optical element to those on the left-hand side (see Fig. 2), thereby automatically accounting for all interference effects accumulated along the way. The transfer matrix will also allow us to calculate the band-gap dispersion relations for an infinite lattice.

A. Dispersion relation for the infinite lattice

We consider a lattice of atomic planes trapped by off-resonance lasers, spaced in its equilibrium configuration according to Eq. (9). The transfer matrix for a single period is given by the product of the transfer matrix across the boundary of an atomic plane and free propagation for a distance d,

$$M=\frac{1}{t}\begin{bmatrix} t^2-r^2 & r \\ -r & 1 \end{bmatrix}\begin{bmatrix} e^{ikd} & 0 \\ 0 & e^{-ikd} \end{bmatrix} =\begin{bmatrix} (1+i\zeta)e^{ikd} & i\zeta e^{-ikd} \\ -i\zeta e^{ikd} & (1-i\zeta)e^{-ikd} \end{bmatrix}, \tag{10}$$

where we have used the single-plane reflection and transmission coefficients given in Eq. (3). For any transfer matrix, the reflection and the transmission coefficients associated with the entire element are

$$r_M=\frac{M_{12}}{M_{22}},\quad t_M=\frac{1}{M_{22}}, \tag{11}$$

as is easily verified for the special case of matrix Eq. (10). We can gain further physical insight by expressing the single-period matrix in a simple form. Given that $\det(M)=1$, its eigenvalues can be written as $m_\pm=e^{\pm i\Theta}$, where Θ is in general a complex number defined by

$$\cos\Theta\equiv\frac{\mathrm{Tr}(M)}{2}=\cos(kd)-\zeta\sin(kd)\ . \tag{12}$$

The matrix can thus be written as

$$M=e^{i\Theta A}=(\cos\Theta)I+i(\sin\Theta)A\ , \tag{13a}$$

$$A=\frac{1}{\sin\Theta}\begin{bmatrix}\zeta\cos(kd)+\sin(kd) & \zeta e^{-ikd}\\ -\zeta e^{ikd} & -\zeta\cos(kd)-\sin(kd)\end{bmatrix}, \tag{13b}$$

with I the 2×2 identity matrix, $\mathrm{Tr}(A)=0$, $A^2=1$, and eigenvalues of A, $a=\pm1$. Eigenvectors of M (and thus any power of M) are the Bloch states of the periodic structure (in the infinite lattice limit) and the parameter Θ gives the corresponding quasimomentum $q=\Theta/d$.

For a real nondispersive polarizability $\zeta=\tan\phi$, the problem is reduced to the Kronig-Penney model and Eq. (12) is the familiar transcendental equation linking the Bloch quasimomentum to its frequency (energy) $\cos\Theta=\cos(kd+\phi)/\cos(\phi)$ [14], with forbidden energies associated with imaginary Θ. Inside the gap the imaginary part of Θ determines the extinction coefficient, so that the extinction length is given as $L_{\mathrm{ext}}=d/[2\,\mathrm{Im}(\Theta)]$. This situation must be contrasted to the case of realistic atoms with a complex polarizability. Here the phase Θ always is complex, due to the scattering losses into nonparaxial modes, and the interpretation of Θ is generally not as simple. In particular, for an atomic transition of linewidth γ excited by a probe detuned from resonance by $\delta=\omega_{\mathrm{probe}}-\omega_{\mathrm{atom}}$, the complex parameter ζ, Eq. (3b), is given by

$$\zeta=\zeta_0\left[\frac{-2\delta/\gamma+i}{1+4\delta^2/\gamma^2}\right]=\tan\phi+i\frac{\eta\sigma}{2}\ , \tag{14}$$

where η is the surface density of atoms,

$$\sigma(\delta)=3\frac{\lambda^2}{2\pi}\left[\frac{1}{1+(2\delta/\gamma)^2}\right] \tag{15}$$

is the absorption cross section for an atomic transition with Clebsch-Gordan coefficient equal to one,

$$\tan\phi=-\frac{\delta}{\gamma}\eta\sigma(\delta) \tag{16}$$

gives the phase shift due to the reactive component of the dipole response, and

$$\zeta_0=\frac{\eta\sigma(0)}{2}=\eta\frac{3\lambda^2}{4\pi} \tag{17}$$

is the resonant scattering parameter. We can now identify the contributions to the imaginary part of Θ arising from purely coherent interference and those due to scattering losses by substituting the complex scattering parameter given in Eq. (14) into Eq. (12),

$$\cos\Theta=-\frac{\cos(\Delta kd-\xi\phi_L+\phi)}{\cos(\phi)}+i\frac{\eta\sigma}{2}\sin(\Delta kd-\xi\phi_L)\ . \tag{18}$$

Here ϕ and σ are the phase shift and absorption cross section at the probe frequency, ϕ_L is the phase shift at the lattice laser frequency, the detuning of the probe from the lattice laser is given by $\Delta k=k-k_L$, and k_Ld is set by the lattice equilibrium condition Eq. (9).

As we said earlier, the band-gap frequencies are characterized by an imaginary quasimomentum, in the absence of scattering losses. Thus, setting $\sigma=0$ in Eq. (18) yields the conditions

$$\cos[\Delta kd-\xi\phi_L+\phi(\delta)]>\cos[\phi(\delta)]\ ,$$

(inside the band gap), (19a)

$$\cos[\Delta kd-\xi\phi_L+\phi(\delta)]<\cos[\phi(\delta)]$$

(outside the band gap). (19b)

Note that for either red or blue detuning, the lattice frequency corresponds to one edge of the band gap ($\phi=\phi_L$, $\Delta k=0$), in which case $\mathrm{Re}[\cos(\Theta)]=-1$. This frequency corresponds to the edge of the Brillouin zone. We thus arrive at the resolution of the paradox stated in Sec. II. The self-consistent solution to the problem of atoms trapped in a standing wave is a structure such that the lattice lasers lie exactly at the edge of the band gap. At this frequency, counterpropagating fields, each injected with the same phase at the incident planes of atoms (as is the case for the lattice laser beams), will fill the lattice as a uniform unattenuated standing wave so that this light is not expelled by the atoms. For frequencies inside the gap, the fields will be attenuated. Because the band-gap frequencies are defined in the absence of atomic absorption, in general the interpretation of the imaginary part of Θ as the extinction coefficient is valid only for frequencies such that the real part of the atomic polarizability is much larger than the imaginary part and for sufficiently long lattices, as we will see below.

The band-gap dispersion relation is governed by two effects: changes in the propagative phase Δkd characterized by the time of flight between planes and changes in the single-plane reflectivity due to the strong frequency dependence of the local atomic response characterized by the natural linewidth. Since $\gamma d/c\ll1$, the former effect can be neglected for small detunings on the order of a few γ. Since all phase shifts are small we can approximate Eq. (18) for the case of red detuning,

$$\Theta_{\mathrm{red}}\approx\pi+2\sqrt{\phi_L(\phi_L-\phi)-i\phi_L\eta\sigma/2}\ , \tag{20}$$

with Δk set to zero. According to Eq. (19), probe frequencies such that $\phi(\delta)>\phi_L$ will be inside the gap. Because of the resonant response given in Eqs. (15) and (16), one band edge is exactly at the lattice frequency and the other at a probe detuning $\omega_{\mathrm{probe}}-\omega_{\mathrm{atom}}=\gamma^2/(\omega_{\mathrm{lattice}}-\omega_{\mathrm{atom}})\approx0$ (i.e., this probe detuning has a magnitude much less than γ for far-off-resonance lattice lasers). The gap frequencies thus extend over the range between the lattice laser frequency and the atomic resonance $\omega_{\mathrm{lattice}}<\omega_{\mathrm{gap}}<\omega_{\mathrm{atom}}$ [see Fig. 3(a)]. In contrast, for a lattice detuned to the blue of resonance, to leading order both propagative phase shifts Δkd as well as dispersion in the atomic response $\phi(\delta)$ must be taken into account to establish the boundaries of the band gap. For small phase shifts, Eq. (18) can be approximated as

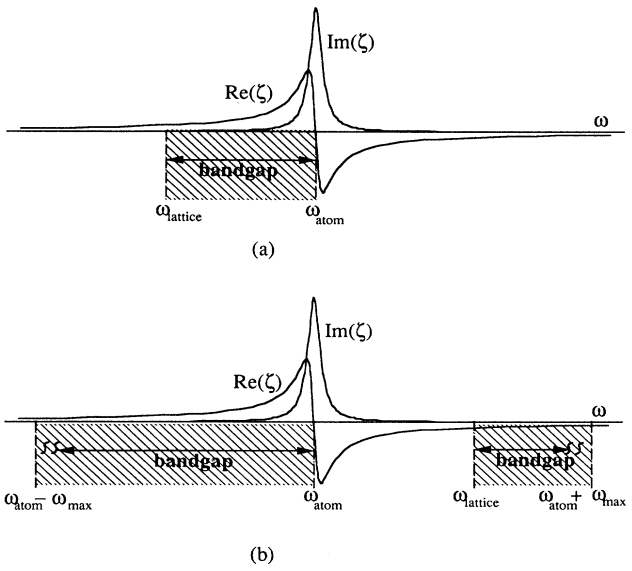

FIG. 3. The frequencies spanned by the photonic band gap are shown in hash marks beneath the dispersion curves of the real and the imaginary parts of the single-atom polarizability α. For the case of the red detuned lattice (a), the band gap extends between the lattice frequency and atomic resonance. For blue detuning (b), the band gap is not continuous, extending over probe detuning between $\pm\Delta\omega_{\max}$ [Eq. (22)], but with frequencies between that lattice laser and the atomic resonance excluded. Typically, $\Delta\omega_{\max}$ is on the order of hundreds of atomic linewidths.

$$\Theta_{\text{blue}} \approx \pi + \sqrt{\Delta kd(\Delta kd + 2\phi) + i\Delta kd\,\eta\sigma}\ . \tag{21}$$

In this case the band-gap frequencies are determined by the condition $\Delta kd > -2\phi(\delta)$. Because of the frequency dependence of ϕ, the band gap is not continuous. In the limit of probe detuning far from the atomic resonance, where Eq. (16) can be approximated by $\phi(\delta) \approx -\zeta_0(\gamma/2\delta)$, the condition (19) for a blue lattice yields the maximum and the minimum edges of the band gap, symmetrically about atomic resonance

$$|\Delta\omega_{\max}| = \left[\frac{\zeta_0\gamma\omega_{\text{atom}}}{\pi}\right]^{1/2}\ . \tag{22}$$

It also follows from Eq. (21) that there is a band edge at the lattice laser frequency and another almost exactly at atomic resonance. Thus the situation for blue-detuned lattices is nearly complementary to the red-detuned case. For blue detuning the band gap extends over two regions $\omega_{\text{atom}} - \Delta\omega_{\max} < \omega_{\text{gap}} < \omega_{\text{atom}}$ and $\omega_{\text{lattice}} < \omega_{\text{gap}} < \omega_{\text{atom}} + \Delta\omega_{\max}$, with frequencies between the atomic resonance and the lattice laser excluded from the gap. For red-detuned lattices, it is exactly this narrow range that constitutes the band gap [see Fig. 3(b)]. The band-gap dispersion relations $\text{Re}[\Theta(\delta)]$ and $\text{Im}[\Theta(\delta)]$ for the case of the cesium $D2$ $6S_{1/2}(F=4) \rightarrow 6P_{3/2}(F'=5)$ resonance are shown in Fig. 4 for both the red and the blue detuned lattices. Note that Θ is always complex due to the imaginary part of ζ.

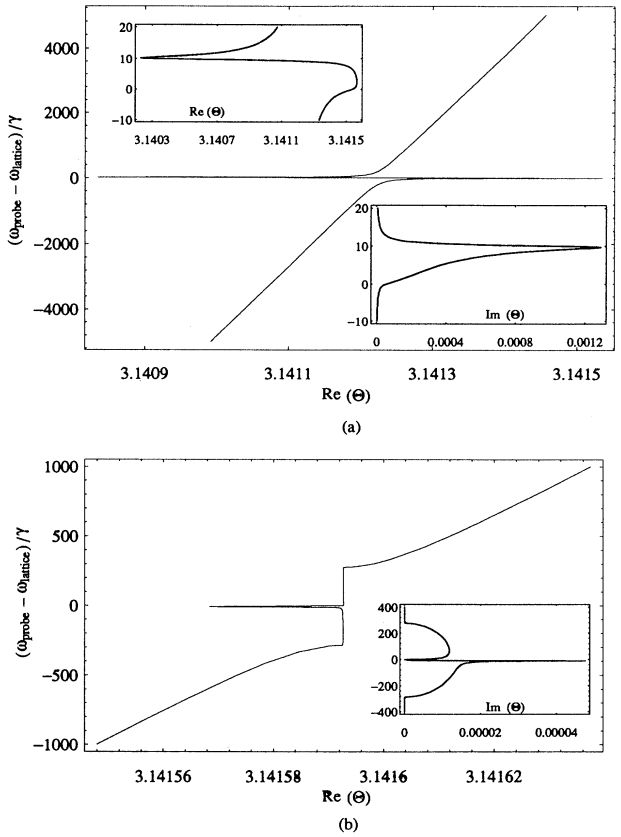

FIG. 4. The one-dimensional band gap dispersion relation $(\omega_{\text{probe}} - \omega_{\text{lattice}})/\gamma$ vs $\text{Re}(\Theta)$ is plotted for lattice lasers trapping Cs atoms with mean density 10^{11} cm^{-3}, (a) detuned to the red by 10γ and (b) detuned to the blue by 10γ. $\Theta = qd$ with q the photon quasimomentum and d the lattice constant. The band gap is exhibited at the edge of the first Brillouin zone $\text{Re}(\Theta) = \pi$ over frequencies in which $\text{Im}(\Theta)$ is large. Far from the gap the dispersion relation is nearly linear as expected for photons. For the case of red detuning (a), the band gap extends between the lattice frequency and atomic resonance shown in detail in the inset in the upper left-hand corner. The imaginary part of Θ near the band gap region is shown in the bottom right inset of (a). For blue detuning (b), the band gap is not continuous extending over probe detuning between $\pm\Delta\omega_{\max} = \pm 280$, but with frequencies between the lattice laser and the atomic resonance excluded. The imaginary part of Θ near the gap is shown in the inset to (b). Distortions to these curves in comparison to those familiar in solid-state physics arise from the rapid dependence of the local atomic polarizability with frequency near the atomic resonance. The imaginary part of this polarizability leads to a small imaginary part in Θ even outside the band gap.

B. Reflection and transmission from a finite lattice

Having determined the character of the band gap associated with the infinite lattice, we return to examine the reflection and the transmission through a finite lattice. The transfer matrix for a lattice of n periods is given simply as the nth power of Eq. (13a),

$$M^n = e^{in\Theta A} = \cos(n\Theta)I + i\sin(n\Theta)A\ . \tag{23}$$

Using Eqs. (11) and (23), the total reflection and transmission coefficients are given by

$$r_n=\frac{(M^n)_{12}}{(M^n)_{22}}=\frac{i\sin(n\Theta)A_{12}}{\cos(n\Theta)+i\sin(n\Theta)A_{22}}=\frac{-i\zeta e^{-i(\Delta kd-\xi\phi_L)}}{\sin\Theta\cot(n\Theta)+i\sin(\Delta kd-\xi\phi_L)+i\zeta\cos(\Delta kd-\xi\phi_L)}\ , \tag{24a}$$

$$t_n=\frac{1}{(M^n)_{22}}=\frac{1}{\cos(n\Theta)+i\sin(n\Theta)A_{22}}=\frac{\sin(\Theta)}{\sin\Theta\cos(n\Theta)+i\sin(n\Theta)[\sin(\Delta kd-\xi\phi_L]+\zeta\cos(\Delta kd-\xi\phi_L)]}\ . \tag{24b}$$

These are the fundamental equations of our analysis, which we will study in various regimes.

In order to gain some physical intuition into the expected behavior of the reflection curves as a function of probe detuning, we must establish the relevant length scales. The relative strength of the probe attenuation due to local scattering and that arising from global interference is central to the physics, the former characterized by the absorption coefficient $\eta\sigma$ and the latter by the band-gap attenuation coefficient $2\,\mathrm{Im}(\Theta)$. The full range of frequencies that define the photonic band gap arises from interference between waves multiply reflected from the atomic planes. This should be distinguished from "kinetic" Bragg scattering, which arises from waves singly scattered from each plane. We will see that the curve of reflection vs the probe frequency exhibits distinctly different character in these different regimes.

For an optically thin lattice, the probability of multiple scattering is negligible. In this case the small difference in the periodicity of the red and the blue lattices has little effect on the probe propagation. The reflected light is then characterized by the interference of the resonance fluorescence spectrum of each individual atom. Because the probe is operating in the low-intensity regime, the radiation pattern can be understood by considering a collection of classically oscillating dipoles, thereby recovering the familiar Bragg scattering of a lattice. The optically thin lattice is characterized by $n\ll 2/\eta\sigma$, in which case Eq. (24a) can be approximated as

$$r_n\approx in\zeta\Longrightarrow|r_n|^2\approx n^2\frac{\zeta_0^2}{1+4\delta^2/\gamma^2}\ . \tag{25}$$

The reflection curve is the Lorentzian response of an individual atom peaked at the atomic resonance and enhanced by n^2 over the single-plane reflectivity Eq. (3a). The parameters associated with this regime are described in more detail in the following section and an example is shown in Fig. 5(a).

As the lattice grows so that it is no longer optically thin on resonance, but still short compared to the band-gap attenuation length at gap center [we assume that at gap center $\mathrm{Re}(\zeta)\gg\mathrm{Im}(\zeta)$, so that the interpretation of Θ is clear], the behavior of the reflection spectrum changes. Here we see the effects of scattering losses, but the lattice is still too small to exhibit the effects of multiple reflections. In this regime $n\eta\sigma\approx 1$, but $n|\Theta-\pi|\ll 1$, so $\cot(n\Theta)\approx 1/n\Theta$ and Eq. (24a) is approximated by

$$r_n\approx\frac{in\zeta}{1-in\zeta}\Longrightarrow|r_n|^2\approx\frac{n^2\zeta_0^2}{(1+n\zeta_0)^2+4\delta^2/\gamma^2}\ . \tag{26}$$

The result is a broadened Lorentzian peaked at resonance, with a rms width $\delta\omega\sim(1+n\zeta_0)\gamma$ [an example is given in Fig. 5(b)]. The broadened peak arises because, when compared to the regime described by Eq. (25), there is a larger probability for a single plane to scatter off-resonance radiation, which can interfere coherently from plane to plane. The lattice is still optically thin to this off-resonance radiation, whereas a larger fraction of the radiation with frequencies closer to resonance is lost to absorption, resulting in a "saturation" of the peak reflectance and a broadening of the wings.

As n increases, the lattice grows large enough that multiple scattering is non-negligible and the difference between red- and blue-detuned lattices becomes apparent. In this regime the peak reflection shifts away from atomic resonance and begins to move towards the gap center. For the case of a red-detuned lattice, the center of the gap is halfway between the lattice frequency and resonance. Given the detuning dependence of Eq. (16), the phase shift at this point is $\phi_{\mathrm{center}}=2\phi_L$ and the corresponding band-gap extinction coefficient is given by Eq. (20) with $\sigma=0$,

$$\kappa_{\mathrm{red}}=2\,\mathrm{Im}(\Theta_{\mathrm{center}})\approx 4\,\mathrm{Im}[\sqrt{\phi_L(\phi_L-\phi_{\mathrm{center}})}]=4\phi_L\ . \tag{27}$$

In order to observe large reflection over the entire band gap, the finite lattice must be long compared to this extinction length d/κ. For probe frequencies such that $\mathrm{Re}(\zeta)\gg\mathrm{Im}(\zeta)$, then as $n\to\infty$ the transmission coefficient (24b) is approximated by

$$\lim_{n\to\infty}t_n=2e^{-n\kappa/2}\frac{-i\sinh(\kappa/2)}{-i\sinh(\kappa/2)+\sin(kd)+\zeta\cos(kd)} \tag{28}$$

and at gap center $|t_n|^2\to 4e^{-2n\kappa}$. Thus in this regime d/κ manifestly appears as the coherent extinction length for propagation inside the band gap. For blue detuning, the band gap is not continuous. The center of each of the gap regions will occur at detunings of approximately $\delta_{\mathrm{probe}}=\pm\omega_{\max}/2$, set by Eq. (22). Clearly, at such large detunings the atomic response is very weak and the corresponding band-gap attenuation coefficient κ_{blue}, as set by Eq. (21), will be very small. We therefore expect that the multiple-reflection regime will be more accessible for red-detuned lattices.

When the lattice length becomes large compared to d/κ the reflection is large over the entire stop band, eventually approaching its infinite limit. For the case of red detuning, since $\mathrm{Im}(\Theta)>0$, $\cot(n\Theta)\to -i$ as $n\to\infty$ and Eq. (24a) can be approximated as

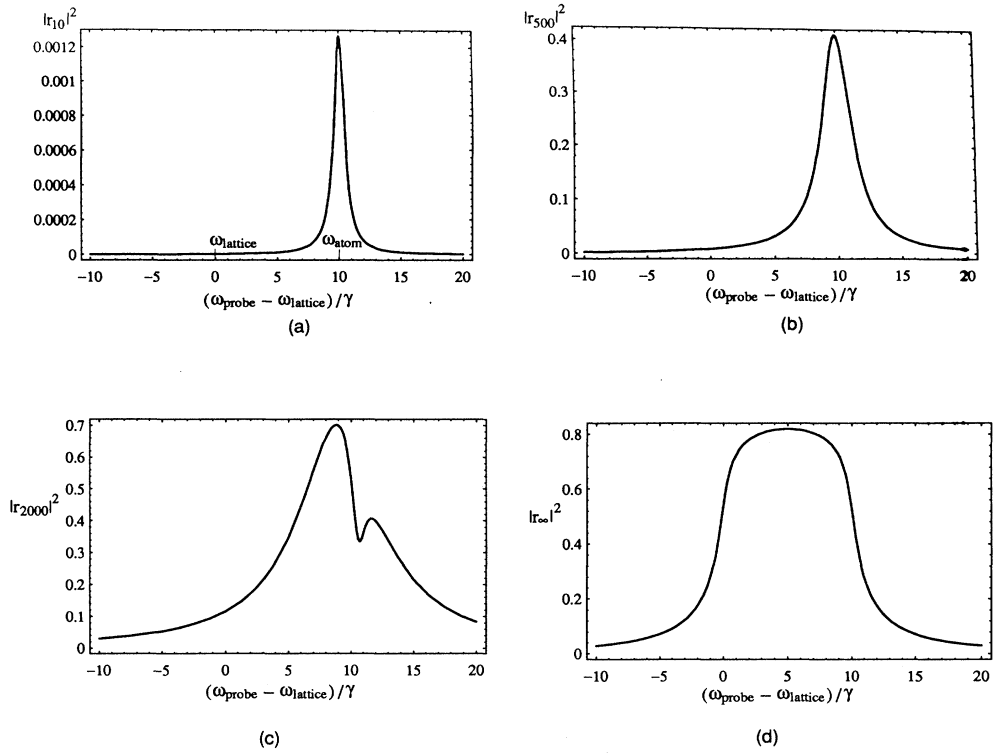

FIG. 5. The absolute square of the reflection coefficient as a function of $(\omega_{\text{probe}}-\omega_{\text{lattice}})/\gamma$ is plotted for a lattice of Cs atoms with mean density 10^{11} cm^{-3} trapped by laser beams detuned to the red of resonance by $\delta_{\text{lattice}}=-10\gamma$ and for various numbers of atomic planes n. For $n=10$ (a), the lattice is optically thin at resonance and the resulting reflection spectrum is the same as that of a single plane Lorentzian enhanced by a factor $n^2=100$ [Eq. (25)]. For $n=500$ (b), the lattice is optically thick at resonance, but short compared to the mean free path for multiple scattering, resulting in a broadened Lorentzian [Eq. (26)]. For $n=2000$ (c), multiple reflections occur, leading to large reflection over a wider range of frequencies, and interference effects give rise to a band edge characterized by the small dip in reflection at resonance. In the infinite lattice limit [Eq. (29) shown in (d)], reflection is large over the entire band gap, reaching a maximum value of 83% at the gap center [Eq. (30)].

$$\lim_{n\to\infty} r_n = \frac{\zeta}{-(\Theta-\pi)+2\phi_L-\zeta} = \frac{\zeta}{-2\sqrt{\phi_L(\phi_L-\zeta)}+2\phi_L-\zeta} \tag{29}$$

[see Fig. 5(d)]. Note that if ζ were purely real, we would have $\zeta=\phi$; also note that the infinite lattice reflection coefficient inside the gap ($\phi>\phi_L$) is a pure phase factor, corresponding to perfect reflection, as expected. The imaginary part of ζ corresponds to a loss mechanism so that, even for an infinite lattice, reflection will not be unity at the gap center. We can estimate the maximum reflection coefficient at the center of the band gap $\omega_{\text{probe}}-\omega_{\text{atom}}=(\omega_{\text{lattice}}-\omega_{\text{atom}})/2\equiv\delta_L/2$. Denoting quantities at the band-gap center by the subscript c and those at the lattice frequency by L, using Eqs. (14) and (20) we find $\zeta_c\approx 2\phi_L(1-i\gamma/\delta_L)$ and $\Theta_c-\pi\approx i2\phi_L(1-i\gamma/2\delta_L)$ for off-resonance lattice frequencies, so that Eq. (29) becomes

$$r_{n\to\infty,c}\approx\frac{2\delta_L-i\gamma}{-2i(\delta_L-\gamma)+\gamma}$$

$$\Rightarrow |r_{n\to\infty,c}|^2\approx\frac{4\delta_L^2+\gamma^2}{4(-\delta_L+\gamma)^2+\gamma^2}\approx\frac{-\delta_L}{-\delta_L+2\gamma}\,. \tag{30}$$

In order to see near unit reflection at the gap center we must have $-\delta_L\gg 2\gamma$. As the lattice laser is tuned closer to the atomic resonance, the imaginary part of the dipole response becomes significant at gap center. Absorption losses then reduce multiple scattering and the resulting structure will act less like a perfect stop band. However, when the lattice is not very far from resonance, fewer planes will be required for the probe laser to enter the "infinite" lattice regime since the band-gap extinction coefficient characterized by ϕ_L is larger. In the next section we will explore the viability of these different regimes in the laboratory.

IV. NUMERICAL EXAMPLES

A. Red-detuned lattice lasers

Consider a one-dimensional lattice of laser-cooled cesium atoms created by counterpropagating identical frequency laser beams, having orthogonal linear polarizations (the lin⊥lin geometry), detuned to the red of the $6S_{1/2}(F=4)\rightarrow 6P_{3/2}(F'=5)$ ($D2$, 852 nm) resonance. In the absence of the atoms, the field can be decomposed into two standing waves of opposite circular polarization, displaced from each other by $\lambda/4$. For the case of red detuning, the spatial dependence of the resulting light-shift potentials and optical pumping rates act in concert to cool and trap the atoms in thin slabs perpendicular to the direction of the lasers, by the process of polarization-gradient Sisyphus cooling [15]. Observations of resonance fluorescence spectra [2] and Raman spectroscopy [1] exhibit strong Lamb-Dicke narrowing, indicating a localization of the atomic slabs to a small fraction of the optical wavelength (a localization better than $\lambda/15$ was reported by Jessen *et al.* for a lattice of rubidium atoms [2]).

In a laboratory realization, atoms are precooled in a magneto-optical trap (MOT), with densities of $N\approx 10^{11}$ cm^{-3}. The MOT fields are then turned off and the lattice beams are turned on. Atoms are trapped at the antinodes of circular polarization where they are optically pumped into the "stretched" Zeeman sublevels ($M_F=\pm F$), with planes of alternate sign of M_F separated by approximately $\lambda/4$. Assuming near perfect one-dimensional trapping, the surface density of atoms in a slab is approximated as $\eta=N\lambda/4=2\times 10^6$ cm^{-2}. The exact equilibrium positions of the trapped planes of optically pumped atoms associated with each circularly polarized standing wave can then be analyzed as in Sec. II, leading to a self-consistent solution [Eq. (9)] for each. By probing this lattice with σ_+ polarization, the scattering rate of photons by atoms pumped into $M_F=-F$ will be $\frac{1}{45}$ that of the rate for atoms pumped into $M_F=F$, due to their respective Clebsch-Gordan coefficients, so we will neglect the former atoms in evaluating the probe response. The remaining atoms and fields then constitute the simple picture of polarized atoms trapped in a standing wave as described in Sec. II.

In Fig. 5 we plot the square of the reflection coefficient [Eq. (24a)] as a function of probe frequency for a lattice laser detuning $\delta_L=-10\gamma$ and in Fig. 6 for $\delta_L=-3\gamma$. We see that the behavior of the reflection spectrum depends strongly on the number of planes n (the length of the lattice is $L\approx n\lambda/2=0.43n$ μm) as discussed in Sec. III. For the parameters at hand, the polarized atoms present a resonant scattering constant $\zeta_0=3.7\times 10^{-3}$. The optically thin regime is characterized by $n\zeta_0\ll 1$ or $n\ll 270$. The reflected intensity is a Lorentzian peaked at atomic resonance, enhanced by the factor n^2 over that reflected from a single plane and a factor n over the intensity reflected from a sample of planes with a random spacing (a situation that well approximates a randomly ordered gas of equal average density when the average spacing between atoms is greater than the optical wavelength). This behavior is seen in both Figs. 5 and 6 for $n=10$ or a lattice length of 4.3 μm, where the reflected intensity is already 0.13% of the probe. In the regime de-

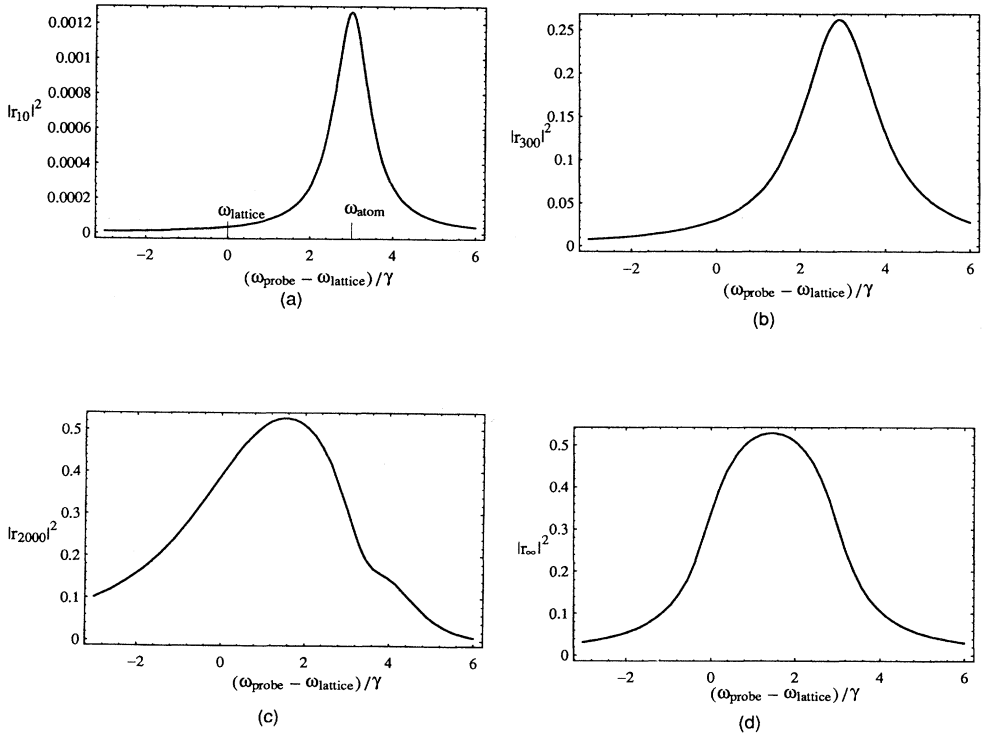

FIG. 6. Same as Fig. 4, but for a lattice laser detuning $\delta_{lattice}=-3\gamma$. For lattices too short to see multiple reflections, (a) $n=10$ and (b) $n=300$, the reflection spectrum is independent of the lattice laser detuning [a change in lattice detuning causes only a small change in the spacing between atomic planes according to the self-consistent solution Eq. (9)]. For $n=2000$ (c) we are already near the infinite lattice limit (d). For lattice lasers closer to resonance, losses reduce reflection inside the band gap, but resonance enhancement of the polarizability allows access to the multiple-scattering regime for shorter lattices.

scribed by Eq. (27), the lattice is no longer thin at the atomic resonance, but is still short compared to the mean free path for multiple scattering, corresponding to lattice lengths such that $1/\xi_0 < n \ll 1/4\phi_L$. The scattering phase shift at the lattice laser detuning $\delta_L = -10\gamma$ is $\phi_L = 1.85 \times 10^{-4}$ with the corresponding band-center attenuation length $\kappa^{-1} = 1350$ planes $= 580$ μm and for $\delta_L = -3\gamma$, $\phi_L = 6.15 \times 10^{-4}$ with $\kappa^{-1} = 407$ planes $= 174$ μm. Examples of broadened Lorentzians in this regime are shown in Fig. 5(b) with $n = 500$, corresponding to a lattice length $L = 213$ μm, where the peak reflection given by Eq. (4.2) is 42% at the atomic resonance, and in Fig. 6(b) with $n = 30$, $L = 150$ μm, and peak reflectivity 26%. For lattices longer than $1/4\phi_L$, multiple scattering is no longer negligible and reflection is large over the full range of the band-gap frequencies. The peak reflectance shifts away from atomic resonance towards the center of the gap. Eventually we approach the infinite limit approximated by Eq. (29), with the peak value given by Eq. (3.24). For $\delta_L = -10\gamma$, this requires very large lattices ($L \gg 580$ μm), giving a maximum reflection of 83%. In contrast, for a lattice laser detuning of $\delta_L = -3\gamma$, the peak reflectance at gap center is 53% and the band edges are less sharp since scattering losses are substantial over the entire band gap. On the other hand, the reflected intensity is significant over all frequencies in the band gap when $L > 150$ μm and approach the infinite limit for L on the order of 500 μm.

For large lattices, exactly at the edge of the band gap as defined by Eq. (19), the reflection coefficient can be quite large ($> 50\%$). This seems to be in contradiction to the self-consistent solution, which we stated allows for the existence of unattenuated lattice laser beams. It must be emphasized that the reflection coefficients calculated here are for a probe beam injected into the lattice only in *one* direction. In that case one can show that for a probe frequency exactly at band edge, the field inside the finite lattice consists of a standing wave with an algebraically decaying envelope (in the absence of absorption) together with a small traveling-wave component that represents the transmitted field. The trapping configuration corresponds to *two* lasers incident from opposite sides of the lattice with the same phase at the input planes. In that case one can show that the steady-state solution is indeed a uniform *unattenuated* pure standing wave.

B. Blue-detuned lattice lasers

Examples of the reflection curve for a lattice created with a laser detuned ten linewidths to the blue of the atomic resonance are shown in Fig. 7. Such an optical lattice cannot be formed from the usual polarization-

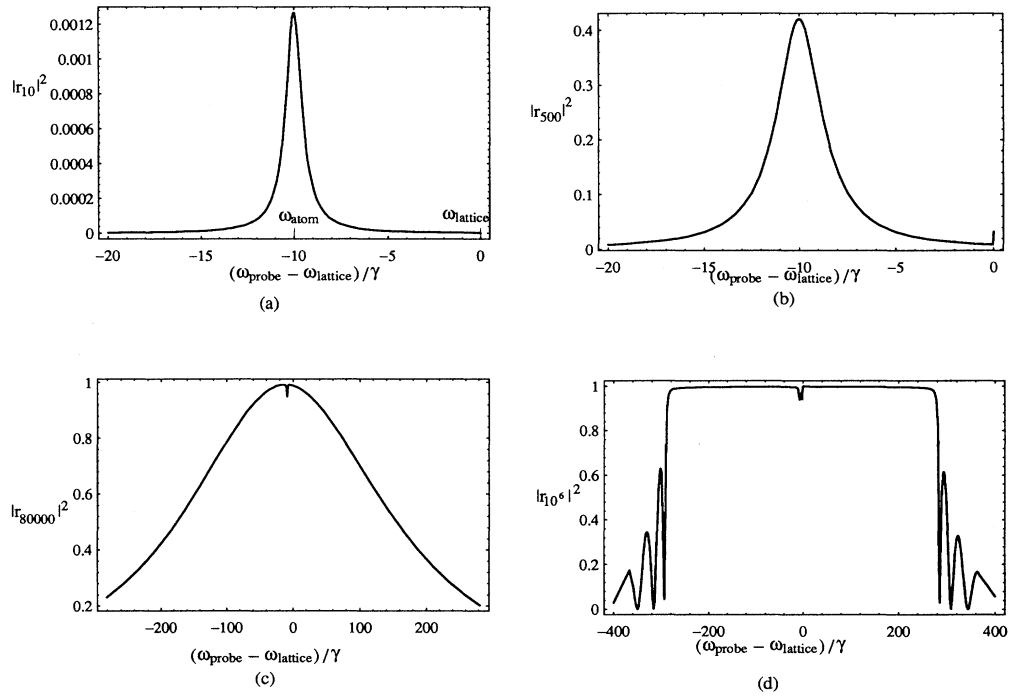

FIG. 7. Same as Fig. 4, but for a blue lattice laser detuning $\delta_{lattice} = +10\gamma$. For lattices (a) $n = 10$ and (b) $n = 500$, the reflection spectrum is the same as that plotted in Figs. 5(a) and 5(b), since multiple scatterings are negligible. For blue detuning the band-gap extinction length is much longer than that for red-detuned lattices and therefore one requires long lattices to see multiple reflections [e.g., $n = 8 \times 10^4$ (c)]. For $n = 10^6$ (d), the reflection spectrum approaches the infinite limit, with near unity reflection inside the noncontinuous band gap extending between $\pm\Delta\omega_{max} = \pm 280\gamma$ [Eq. (22)], but with frequencies between the atomic resonance and the lattice frequency excluded, as is revealed by the dip in reflectivity seen in (d) near zero detuning. Notice the resemblance between this curve and the reflection spectrum for a multilayer lossless dispersionless dielectric.

gradient Sisyphus mechanism on an atomic $J \rightarrow J+1$ transition. For the purpose of illustration here we will assume that one can produce a blue-detuned trapping lattice and do not concern ourselves with the exact mechanism of loading it. Recall that within our model, we neglect the processes that lead to laser cooling or heating, so that the sole effect of the detuning of the lattice laser beams is to determine the equilibrium spacing between the atomic planes according to the self-consistent solution Eq. (9) [16]. The small difference in the lattice periodicity nonetheless has dramatic effects on the reflection spectrum.

As in the red-detuned case, the reflection curves shown in Fig. 7 exhibit the expected behavior as a function of lattice length. For thin lattices the reflection curve resembles the single-atom resonance fluorescence spectrum. When multiple scattering is negligible, the reflection spectrum is independent of the lattice laser detuning (sign and magnitude). Evidence of the small changes in the atom's equilibrium positions requires many multiple reflections for the probe to accumulate a significant phase shift (e.g., for $n=10$, planes Figs. 5–7 are equivalent). For very long lattices, interference between multiply scattered waves dominates and reflection becomes large over the noncontinuous band gap described in Sec. III. Because the band gap extends over frequencies far from resonance where the atomic response is relatively lossless and nondispersive, the reflection curve closely resembles that observed for multilayer dielectric structures. It must be emphasized that at these large detunings the atomic response is very weak and thus observation of the total stop band would require extremely long lattices, much longer than for red detuning. For the parameters here, the far edges of the gap are given in Eq. (22) by the detunings $\Delta\omega_{\max}=\pm 280\gamma$. At probe detunings at the centers of the two gap regions $\delta_c=\pm\Delta\omega_{\max}/2$, the band-center attenuation length is given by $\kappa^{-1}=1.5\times 10^5$ planes. Observation of strong reflection at this detuning would require a lattice length of $L>6.5$ cm, which would be extremely difficult to achieve experimentally. Notice the small dip in the reflectivity near atomic resonance spanning the frequencies between the atomic resonance and the lattice laser frequency, which are excluded from the photonic band gap. This dip does not bring the reflectivity exactly to zero because of the scattering losses.

C. Comparison with Beer's law

The discussion above concentrated on the reflection spectrum since the observation of a significant fraction of the incident intensity in the reflected beam would be a signature of spatial ordering. We may also consider the behavior of the transmitted beam as a function of the

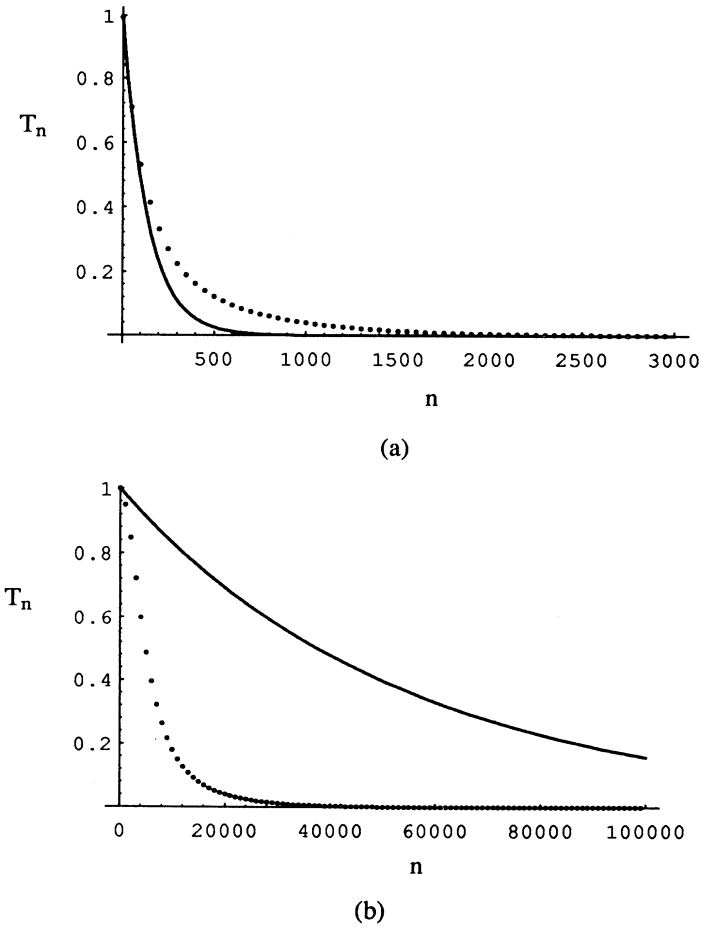

FIG. 8. The transmission coefficient (dotted) curve at the two edges of the band gap: (a) the atomic resonance and (b) at the lattice laser frequency. The parameters of the Cs lattice are given in Sec. IV, trapped by lattice lasers detuned to the red by ten linewidths. Plotted simultaneously in solid curves is Beer's exponential decay law for a disordered gas of the same averaged density. The transmitted intensity in the lattice at atomic resonance (a) is larger than that of the disordered gas, whereas the transmission is less at the lattice frequency (b) due to interference of forward- and backward-scattered waves.

probe detuning. If the gas were disordered, then the transmission coefficient for the intensity would follow Beer's law $T(\delta)=\exp\{-n\eta\sigma(\delta)\}$. In this situation, light that is not transmitted is lost to absorption (scattered into nonparaxial modes) and a negligible fraction is reflected when the density of atoms is small compared to $1/\lambda^3$. In Fig. 8 we plot the absolute square of the transmission coefficient as a function of the sample length, for a lattice created with lasers detuned to the red by ten linewidths [see Eq. (24b)], simultaneously with the prediction given by Beer's law for an equal average density of atoms. We consider probe frequencies at the two edges of the band gap (i.e., at the lattice laser frequency and at the atomic resonance). At the lattice frequency the transmitted intensity is less than Beer's law prediction. This is not surprising since a large fraction of the energy is reflected. On the other hand, at the atomic resonance frequency the transmitted intensity is actually *larger* than it would have been in a disordered gas at the same time that the reflected intensity is substantial. This result appears surprising since one might assume that in traversing the sample, scattering losses are inescapable and thus that Beer's law would set a maximum for the transmitted energy.

The resolution to this problem lies in the coherent interference of the backward-scattered wave, characteristic of spatial ordering of the lattice. In contrast to propagation in a disordered gas, the light propagating in the lattice will have a standing-wave as well as a traveling-wave component. As we pointed out in Sec. III, for a red-detuned infinite lattice, the eigenmodes at the band edges are standing-wave solutions; at the low-frequency edge of the band gap (i.e., at the lattice frequency) there are antinodes at the atomic planes and at the high-frequency edge (i.e., at the atomic resonance) there are nodes at these planes. In a finite lattice there will always be a traveling-wave component so that the eigenmodes at the band edges have neither perfect nodes nor antinodes. Nonetheless, the positions of the minima and the maxima of the intensities are as described above, as is dictated by the self-consistent solution described in Sec. II. The end result is that scattering losses are actually reduced at atomic resonance since the coherent interference reduces the intensity of the field seen at the position of the scatterers; scattering losses are slightly enhanced at the lattice laser frequency since the atoms experience a stronger field. When the lattice grows longer than the band-gap extinction length, scattering losses will always

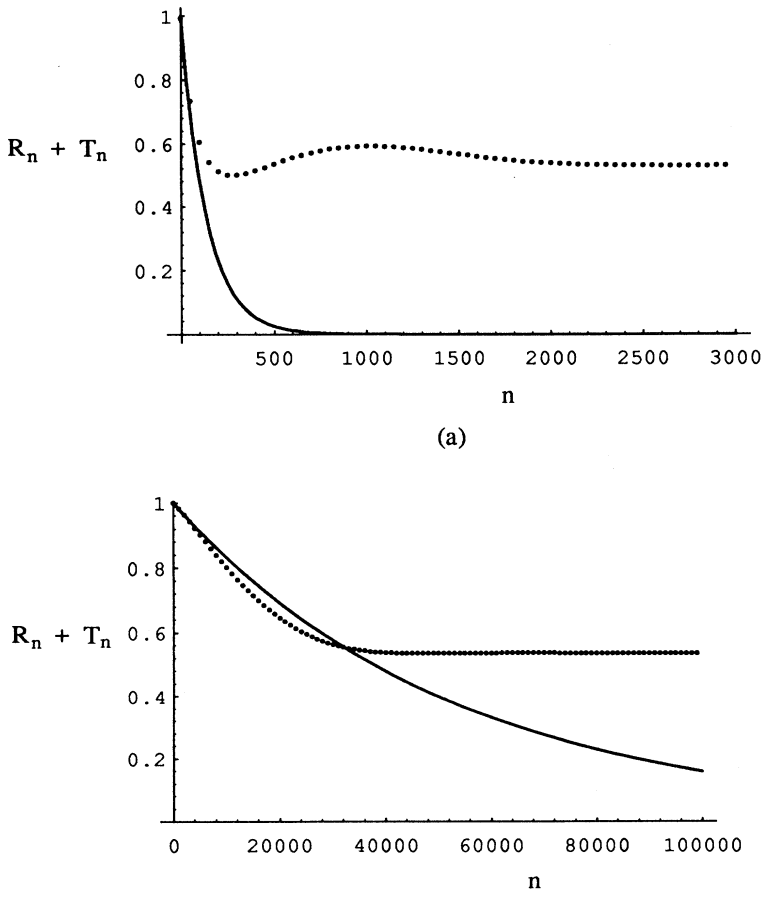

FIG. 9. The total fraction of intensity in the reflected and transmitted beam, R_n+T_n as in Fig. 8, (a) at the atomic resonance and (b) at the lattice frequency. For sufficiently short lattices, the scattering loss in the lattice is smaller than Beer's law prediction, but larger than Beer's law at the lattice frequency because of interference effects described in Sec. IV. When the lattice is much longer than the band gap extinction length, the incident field does not penetrate any deeper into the lattice, so scattering losses saturate, where they tend to 100% in the disordered gas.

be less than they would have been in an equal density disordered gas since the majority of the incident intensity is reflected. The incident field only penetrates the ordered gas to a "skin depth" set by the band-gap extinction length and thus additional planes beyond this length will not result in scattering loss. These results are shown clearly in the plots of the sum $|r_n|^2+|t_n|^2$ as a function of n, presented in Fig. 9. In a disordered dilute gas we would expect $|r_n|^2+|t_n|^2\approx\exp(-n\eta\sigma)$ (since the reflected intensity is negligible). Figure 9(a) reveals the suppression of the total scattering losses at the atomic resonance for lattices short compared to d/κ and Fig. 9(b) shows the slight enhancement at the lattice frequency. For $n\gg\kappa^{-1}$, in the ordered gas most of the incident intensity is reflected and the total scattering losses saturate, whereas in the disordered gas $|r_n|^2+|t_n|^2\rightarrow 0$.

D. Other experimental considerations

At this point we have considered the ideal lattice consisting of infinite atomic planes that are δ-function localized. We now consider how a more realistic geometry would affect the predicted results. Atomic planes with a finite diameter D will scatter a diffraction limited beam with an angular divergence on the order $\beta_{\text{diff}}\approx\lambda/\pi D$. If the off-axis waves are to be effectively scattered, they must lie within the angular width of the Bragg peak β_{Bragg} set by the condition $1-\cos\beta_{\text{Bragg}}\approx 1/nkd$ (excluding multiple scattering) or for small angles $\beta_{\text{Bragg}}\approx(\lambda/\pi nd)^{1/2}$. If we assume that the total volume of atoms is essentially spherical so that the transverse and longitudinal sizes are equal, $D=nd$. Since $D\gg\lambda$, we always satisfy $\beta_{\text{diff}}<\beta_{\text{Bragg}}$ and diffraction effects will not limit the Bragg scattering responsible for the band gap. For $n=2000$, the acceptance angle is approximately $\beta_{\text{Bragg}}\approx 13$ mrad. In addition, the polarization dependence of the scattering for nonnormal incidence does not impose unreasonable collimation constraints on the beam (see the Appendix).

The fact that the atoms are not perfectly localized in planes also has potential for diminishing the strength of the observed band gap. The spread in position of the atoms results in a reduction in the strength of the Bragg scattering in a manner analogous to the effect of a finite slit width in an n-slit diffraction grating [7]. The diffracted peaks are reduced by a factor set by the Fourier transform of the slit function. In previous measurements in a one-dimensional lattice of rubidium [2], the rms localization of the atoms was measured to be $\sim\lambda/15$. Assuming that the center of mass wave functions of the atoms that are deeply bound in the light-shift potential well can be approximated by states of a simple harmonic oscillator, the probability distribution of the atomic position is Gaussian. The Bragg peak will then be reduced by a factor $f=\exp(-4k^2\Delta x^2)$, where $k=2\pi/\lambda$ and $\Delta x=\lambda/15$, or $f=0.5$, a reduction that should not pose any experimental difficulties.

The considerations above indicate that substantial reflection from the optical lattice should be observable in the laboratory. We note that in previous pump-probe Raman spectroscopy experiments on optical lattices [9], off-axis scattering into the direction of maximum Bragg reflection has been observed. These results do not give unambiguous proof of the long-range spatial ordering in the lattice since the scattered beams are produced in the direction for phase-matched four-wave mixing (i.e., phase-conjugate reflection off population or spin gratings). Our proposed experiment differs in the following respects: The frequency difference between the pump and the probe beams is on the order of several natural linewidths, or tens of megahertz, far from any vibrational resonance of atoms trapped in the wells (kilohertz scale). Moreover, the most compelling demonstration of the effect of spatial ordering can be seen in a transient experiment by scattering the probe from the atomic lattice after the lattice laser beams have been turned off. If the atoms were spatially ordered they will remain so for many microseconds due to their extremely low temperature. After a very short time (a few natural lifetimes) all the atoms are in the ground state, so spatial gratings in the ground-excited state *population difference,* irrespective of true spatial ordering of the atomic *positions,* have been removed. Eventually the atoms travel over sufficient distances to wash out the coherent backscattering. According to the discussion above, the Bragg peak will be reduced to 10% when the spread in atomic positions about a plane is $\Delta x=0.12\lambda$. Assuming a temperature associated with three to four recoil velocities $v_{\text{rec}}=\hbar k/M$, or 1–1.5 cm/s, atoms will diffuse over this distance in 7–10 μs. This time scale is much longer than the inverse of the band-gap width and thus should allow full exploration of the curve of reflection vs probe frequency.

Although this experiment can remove four-wave mixing as a possible mechanism for the observed Bragg reflection, we still may not rule out coherent scattering from a "spin grating" created in a cold but spatially homogeneous gas by the local optical pumping associated with the spatially periodic polarization of the optical lattice light field. Propagation of a probe in an optically pumped polarized gas was first studied by Cohen-Tannoudji and Laloë [10(a)] and specialized to a laser cooled sample whose ground state is "optically oriented" by Bezverbnyi, Smirnov, and Tumaikin [10(b)]. In order to distinguish (by the existence or nonexistence of Bragg reflection) the spatial ordering of the atom's internal degree of freedom from a density grating associated with its center of mass position, we must consider higher-dimensional lattices. The spin lattice may be at least partially separated from the atomic-density lattice by an appropriate choice of probe polarization. Such a system is analyzed in the next section.

V. BRAGG SCATTERING IN THREE-DIMENSIONAL LATTICES

Up until this point we have been considering a lattice in which atoms are trapped only along one dimension and randomly distributed in the plane. Atoms can also be trapped in three-dimensional lattices through the interference of multiple laser beams. Bragg scattering then

has potential as a useful tool for studying the long-range and the short-range spatial order of the lattice. We consider a configuration of four linearly polarized beams, represented by the ordered pairs (polarization, wave vectors): $(\mathbf{e}_x, \mathbf{k}_1 = k_\perp \mathbf{e}_y + k_\parallel \mathbf{e}_z)$, $(\mathbf{e}_x, \mathbf{k}_2 = -k_\perp \mathbf{e}_y + k_\parallel \mathbf{e}_z)$, $(\mathbf{e}_y, \mathbf{k}_3 = k_\perp \mathbf{e}_x - k_\parallel \mathbf{e}_z)$, and $(\mathbf{e}_y, \mathbf{k}_4 = -k_\perp \mathbf{e}_x - k_\parallel \mathbf{e}_z)$ with $k_\parallel = k\cos\theta$ and $k_\perp = k\sin\theta$. This geometry can be envisaged as a simple modification of the standard one-dimensional lin⊥lin geometry [6]. Each of the counterpropagating beams is "split" into two beams by an angle θ in directions perpendicular to their polarizations, giving rise to a three-dimensional lattice

$$\begin{aligned}\varepsilon &= [(e^{i\mathbf{k}_1\cdot\mathbf{x}} + e^{i\mathbf{k}_2\cdot\mathbf{x}})\mathbf{e}_x - i(e^{i\mathbf{k}_3\cdot\mathbf{x}} + e^{i\mathbf{k}_4\cdot\mathbf{x}})\mathbf{e}_y]/\sqrt{8} \\ &= \mathbf{e}_- \left[\cos(k_\parallel z)\left[\frac{\cos(k_\perp y)+\cos(k_\perp x)}{2}\right] + i\sin(k_\parallel z)\left[\frac{\cos(k_\perp y)-\cos(k_\perp x)}{2}\right]\right] \\ &\quad - \mathbf{e}_+ \left[\cos(k_\parallel z)\left[\frac{\cos(k_\perp y)-\cos(\mathbf{k}_\perp x)}{2}\right] + i\sin(k_\parallel z)\left[\frac{\cos(k_\perp y)+\cos(k_\perp x)}{2}\right]\right]. \end{aligned} \tag{31}$$

The result is interleaved lattices for each of the two circular polarizations σ_+ and σ_-. Each lattice is centered tetragonal, with the two lattice constants $a_\parallel = \lambda/2\cos\theta$ and $a_\perp = \lambda/\sin\theta$. These polarization lattices give rise to periodic σ_+ and σ_- light-shift potential wells, which can trap and optically pump atoms into the respective stretched states.

Bragg scattering occurs when the difference between the momenta of the probe and scattered photons is a reciprocal-lattice vector. For optical lattices, a primitive basis for these vectors will always be given by the difference between the k vectors of these beams [4]. In the Raman spectroscopy experiments of three-dimensional lattices performed by Grynberg *et al.* [4], a probe counterpropagating against one of the lattice beams results in Bragg reflection along another lattice beam. However, these experiments can equally well be interpreted as phase-matched four-wave mixing. As our goal is to use Bragg scattering as a tool to study the spatial order of the atomic positions, we want to remove this ambiguity by considering experiments in the absence of lattice light, as in the experiment proposed in Sec. IV. As we noted there, even after the lattice laser beams are removed, observation of a reflected beam still would not give unambiguous proof of the spatial order of the atomic positions because of the existence of the "spin lattice" associated with the local polarization of the optical lattice. By a spin lattice we mean a periodic variation in the multipole moments associated with the internal Zeeman state distribution of the atoms (orientation and alignment) [17]. This ambiguity cannot be removed in the one-dimensional (lin⊥lin) case since the spin lattice and the atomic density lattice seen by the probe are always coexistent. In particular, in a one-dimensional lattice the orientation associated with an optically pumped but otherwise homogeneous cold gas in a lin⊥lin field, when averaged over a plane corresponding to a phase front of a probe, will vary periodically in the same way as the hypothesized density distribution of trapped atomic planes. The extra degrees of freedom available in three dimensions allows us to create a system in which these two phenomena can be separated.

Consider scattering a probe propagating in the z direction and linearly polarized (e.g., $\varepsilon_{\text{probe}} = \mathbf{e}_x$). It follows from Eq. (31) that there exists a set of atomic planes that give rise to reflection by Bragg scattering when the wavelength of the probe is $\lambda_{\text{probe}} = \lambda_{\text{lattice}}/(2\cos\theta)$. Since the scattering is minimal except for frequencies near atomic resonance, it is practical to choose $\theta = \pi/3$. All planes perpendicular to z will contain an equal amount of σ_+ and σ_- polarized light, in contrast to the one-dimensional lattice, which has planes with alternating pure helicity. The orientation of the resulting optically pumped atoms averages to zero over these planes. A linearly polarized probe incident in the z direction, containing an equal amount of σ_+ and σ_- polarized light, will therefore not experience a periodic variation in the atomic orientation, which could backscatter the light. In contrast, a true center of mass grating arising from the long-range density correlations of trapped atoms should give rise to substantial coherent backscattering as calculated in the previous sections. Finally, it remains to consider the quadrupole moment (or alignment) of the optically pumped atoms in the field given by Eq. (31). A periodic variation of this parameter, when averaged over the planes perpendicular to the z direction, could also give rise to coherent backscattering, even in the absence of a density grating. Such a calculation is beyond the scope of this article and requires further research, though it seems likely that the average alignment would only weakly scatter the probe in contrast to the strong Bragg scattering predicted for localized trapped atoms. Until such a calculation is done we cannot unambiguously distinguish the observation of Bragg scattering off a lattice of localized atoms from Bragg scattering off a spin lattice.

VI. DISCUSSION

We have seen that an optical lattice can potentially reflect a large fraction of the intensity of a weak probe and that the characteristics of the reflection spectrum vary as a function of the lattice length. In this section we interpret these results in terms of fundamental processes of absorption and emission of photons. For short lattices, the probability of multiple reflections is negligible and thus the reflection spectrum is characterized by the

scattering off a single plane. In that case, the individual atoms spontaneously scatter light according to their dipole response, which is dominated by the imaginary part near resonance. Although these scattering events correspond to spontaneous emission, it is well known that at low intensities the resonance fluorescence is coherent, so we can calculate the expected pattern as if the atoms were classically polarizable particles. Interference in the resonance fluorescence of two trapped Hg^+ ions has previously been observed [18], yielding a classical Young-type two-slit interference pattern. In the lattice geometry, the coherent addition of individual dipole patterns in a plane results in light scattered mainly into the forward and the backward directions (there is some light scattered into nonparaxial modes, which results in a loss) and the spatial ordering of n planes then enhances the reflected wave intensity by n^2. Thus, for thin lattices where multiple scattering can be neglected, it is the imaginary part of the atomic response that dominates. This is revealed in the reflection spectrum seen in plots (a) and (b) in Figs. 5–7.

The imaginary part also gives rise to losses. For a single plane, the intensity not radiated into either the transmitted or reflected beams follows from Eqs. (3) and (14),

$$1-|r_1|^2-|t_1|^2=\frac{\eta\sigma}{1+\eta\sigma+\tan^2\phi+(\eta\sigma)^2/4} . \quad (32)$$

No photons are truly "lost" after propagating through the gas of atoms (i.e., converted to heat in some other form of energy such as phonons); they are only rescattered into nonparaxial modes. Since all the radiated fields are phase coherent, it would seem that the superposition of all the individual dipole patterns in a plane can only have components propagating in the forward or the backward direction. The resolution to this puzzle lies in our simple model of the plane of atoms as a continuous, homogeneous polarizable sheet. Our situation is analogous to the Mie scattering by small lossless dielectric spheres. It is well known that the propagation of light in a gas of such particles can be modeled by a bulk homogeneous medium with a complex index of refraction [11]. The losses represented in Eq. (32) should thus be attributed to the diffuse scattering resulting from the random locations of the atomic positions in the plane, assumed sufficiently sparse that the average number of atoms per area is small compared to the scattering cross section. If the atoms in a single plane are themselves arranged on a regular two-dimensional grid, these "losses" would be attributed to higher-order diffraction peaks.

We therefore conclude that the large reflection over the entire band gap arises from the real part of the atomic response. In Fig. 10 we plot the reflection dispersion curve given by Eq. (24) for the same parameters as in Sec. IV, a lattice detuning of $\delta_L=-10\gamma$, but with the imaginary part of ζ artificially set to zero. Note the resemblance between these curves and those given in Fig. 5 in the long lattice regime. Whereas the artificial system leads to unity reflection inside the band gap, for true atomic response the imaginary part leads to scattering into nonparaxial modes, which prevents the multiple reflections needed to produce a perfect stop band.

In summary, we have shown that an optical lattice can exhibit a one-dimensional photonic band gap due to the long-range periodic ordering of the atomic positions on the scale of the optical wavelength. The backaction of the trapped atoms on the lattice laser beams leads to a self-consistent solution that determines the equilibrium

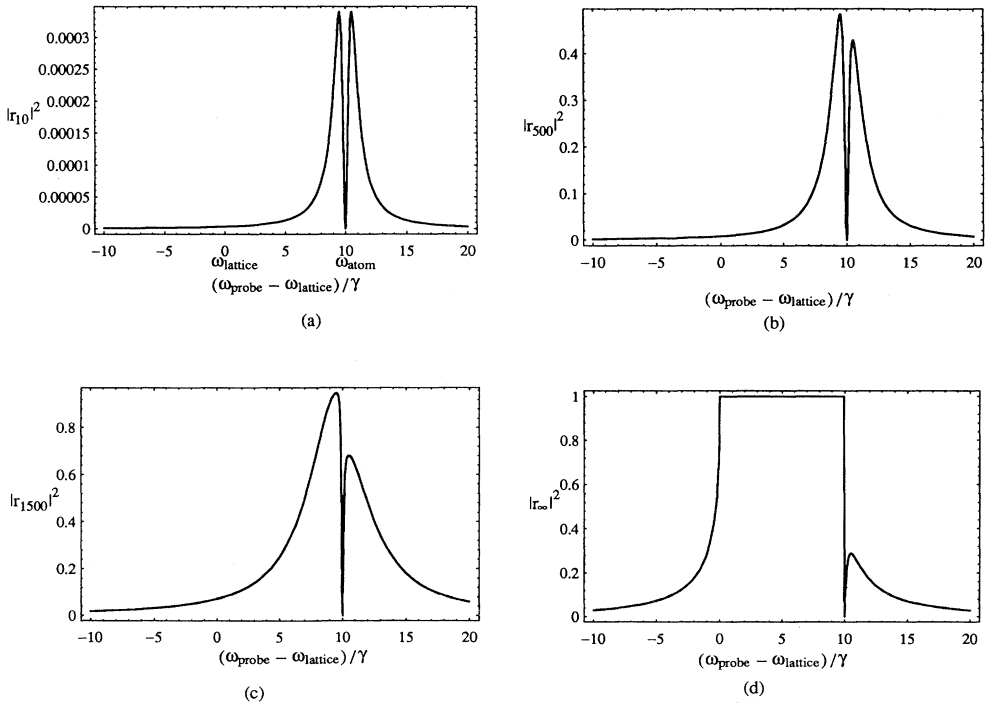

FIG. 10. The absolute square of the reflection coefficient as a function of $(\omega_{probe}-\omega_{lattice})/\gamma$ is plotted for the same parameters as Fig. 5, but with the imaginary part of the atomic polarizability α set to zero. We see the evolution from the thin lattice regime (a) $n=10$ and (b) $n=500$ to multiple reflections (c) $n=2000$ and the infinite lattice (d). In the absence of $\mathrm{Im}(\alpha)$, there are no scattering losses and the lattice acts as a perfect stop band inside the band gap.

positions of the Bragg planes and always has a photonic band edge at the lattice laser frequency. For lattices trapped by red-detuned lasers, the band gap extends from the trapping laser's frequency to atomic resonance. The case of a blue-detuned trapping laser is complementary; the frequencies between resonance and the lattice laser are excluded from the gap. Otherwise the gap extends over a large range, typically on the order of hundreds of atomic linewidths, centered at resonance. We see that the curve of reflected intensity as a function of probe frequency associated with Bragg scattering in a thin lattice follows the Lorentzian resonance fluorescence spectrum of a single atom, whereas the curve becomes distinctly non-Lorentzian in the infinite lattice limit. The transmitted energy also differs in the ordered gas from Beer's exponential attenuation expected for a disordered gas. At atomic resonance, interference between forward- and backward-scattered waves gives rise to standing waves with intensity minima at the atomic planes, thereby suppressing scattering loss (and increasing transmission); the opposite is true at the lattice laser frequency. Finally, we considered Bragg scattering in a three-dimensional lattice.

ACKNOWLEDGMENTS

We gratefully acknowledge P. Jessen, G. Birkl, M. Gatzke, M. Walhout, T. Lucatorto, P. Lett, U. Sterr, and A. Steinberg for many helpful discussions. I.H.D. thanks the NRC/NIST and R.J.C.S. thanks the Niels Stensen Stichting for financial support. This work was partially supported by the U.S. Office of Naval Research and by NSF Contract No. PHY-9312572.

APPENDIX

In this appendix we generalize the reflection and the transmission coefficients of the probe from a plane of atoms to the case of nonnormal incidence in order to determine their sensitivity to the electric-field polarization. Consider a monochromatic wave incident on a plane of polarizable particles at $z=0$ with wave vector $\mathbf{k}=k_x\mathbf{e}_x+k_z\mathbf{e}_z$ and frequency $\omega=c\sqrt{k_x^2+k_z^2}$. Using the symmetry of the problem we can express the fields on the left- and the right-hand sides of the plane by the ansatz

$$\mathbf{E}_L=(\mathbf{E}_0e^{ik_zz}+\mathbf{E}_re^{-ik_zz})e^{ik_xx}\ , \tag{A1a}$$

$$\mathbf{E}_R=\mathbf{E}_te^{ik_zz}e^{ik_xx}\ , \tag{A1b}$$

where $\mathbf{E}_0$, $\mathbf{E}_r$, and $\mathbf{E}_t$ are the vector amplitudes of the incident, the reflected, and the transmitted fields, respectively. These can be expressed in terms of the components in the plane of incidence $\mathbf{u}_p\equiv\cos\theta\mathbf{e}_x-\sin\theta\mathbf{e}_z$, $\mathbf{u}_q\equiv\cos\theta\mathbf{e}_x+\sin\theta\mathbf{e}_z$ and perpendicular $\mathbf{u}_s\equiv\mathbf{e}_y$, with θ the angle of incidence. In general, the atomic response will be birefringent and thus these will not be the eigenpolarizations of the problem. We thus seek the eigenvectors and eigenvalues for transmission through the plane. As in Sec. II, this can be simply calculated through the boundary conditions for propagation. Expressed in terms of the $\{p,q,s\}$ components, the amplitude of the tangential components of the fields in Eq. (A1) at $z=0$ are

$$E_x(z=0_-)=\cos\theta(E_{0p}+E_{rq})\ , \tag{A2a}$$

$$E_x(z=0_+)=\cos\theta E_{tp}\ , \tag{A2b}$$

$$E_y(z=0_-)=E_{0s}+E_{rs}\ , \tag{A2c}$$

$$E_y(z=0_+)=E_{ts}\ . \tag{A2d}$$

These tangential E fields are continuous across the plane, while the induced current sheet results in a discontinuity of the magnetic field, or equivalently the electric-field derivative, which can be determined from Maxwell's equations.

The propagation of the field in the plane of incidence is governed by the wave equation

$$\nabla(\nabla\cdot\mathbf{E})-\nabla^2\mathbf{E}-k^2\mathbf{E}=4\pi k^2\mathbf{P}=4\pi k^2\chi\cdot\mathbf{E}\ , \tag{A3}$$

where χ is the susceptibility tensor. Substituting in the ansatz $\mathbf{E}=\mathbf{E}(z)e^{ik_xx}e^{\pm ik_zz}$, the Cartesian components read

$$\partial_s^2E_x-ik_x\partial_zE_z+k^2E_x=-4\pi k^2\mathbf{e}_x\cdot\chi\cdot\mathbf{E}\ , \tag{A4a}$$

$$(\partial_z^2+k_z^2)E_y=-4\pi k^2\mathbf{e}_y\cdot\chi\cdot\mathbf{E}\ , \tag{A4b}$$

$$-ik_x\partial_zE_x+k_z^2E_z=-4\pi k^2\mathbf{e}_z\cdot\chi\cdot\mathbf{E}\ . \tag{A4c}$$

For atoms optically pumped into the Zeeman sublevel with maximum angular momentum along the z axis, χ can be approximated by the dyadic

$$\chi=\eta\alpha_+\delta(z)\mathbf{e}_+\mathbf{e}_+^*\ , \tag{A5}$$

where α_+ is the polarizability of the pump atom to σ^+ light, η is the density of atoms per unit area, and $\mathbf{e}_\pm=\mp(\mathbf{e}_x\pm i\mathbf{e}_y)/\sqrt{2}$ are the usual unit vectors of circular polarization. The right-hand side of Eq. (A4c) vanishes and the E_z can be eliminated in terms of the E_x. Equations (A4a) and (A4b) become a coupled set of one-dimensional wave equations

$$(\partial_z^2+k_z^2)E_x=-2\pi k_z^2\eta\alpha_+\delta(z)(E_x-iE_y)\ , \tag{A6a}$$

$$(\partial_z^2+k_z^2)E_y=-i2\pi k^2\eta\alpha_+\delta(z)(E_x-iE_y)\ . \tag{A6b}$$

The boundary conditions on the fields and their derivatives are then

$$E_x(z=0_+)-E_x(z=0_-)=0\ , \tag{A7a}$$

$$\partial_xE_x(z=0_+)-\partial_zE_x(z=0_+)=-2\pi k_z^2\eta\alpha_+[E_x(0)-iE_y(0)]\ , \tag{A7b}$$

$$E_y(z=0_+)-E_y(z=0_-)=0\ , \tag{A7c}$$

$$\partial_xE_y(z=0_+)-\partial_zE_y(z=0_+)=-i2\pi k^2\eta\alpha_+[E_x(0)-iE_y(0)]\ . \tag{A7d}$$

Using these and Eq. (A2) we arrive at the transmission coefficient matrix for the p and s components

$$\begin{bmatrix} E_{ip} \\ E_{ts} \end{bmatrix} = \begin{bmatrix} 1+i\frac{\rho}{2}\cos^2\theta & \frac{\rho}{2}\cos\theta \\ -\frac{\rho}{2}\cos\theta & 1+i\frac{\rho}{2} \end{bmatrix} \begin{bmatrix} E_{0p} \\ E_{0r} \end{bmatrix} , \tag{A8a}$$

where

$$\rho \equiv \frac{\zeta}{\cos\theta - i\frac{\zeta}{2}(\cos^2\theta+1)} \tag{A8b}$$

and ζ is defined in Eq. (3b). The transmission eigenvalues and corresponding eigenpolarizations are

$$t_1 = \frac{\cos\theta}{\cos\theta - i\frac{\zeta}{2}(\cos^2\theta+1)} ,$$
$$\mathbf{e}_1 = -\frac{1}{\sqrt{1+\cos^2\theta}}\{\cos\theta\mathbf{u}_p + i\mathbf{u}_s\} , \tag{A9a}$$

$$t_2 = 1 ,$$
$$\mathbf{e}_2 = -\frac{1}{\sqrt{1+\cos^2\theta}}\{\mathbf{u}_p - i\cos\theta\mathbf{u}_s\} . \tag{A9b}$$

Similarly, one finds the reflection coefficients for these eigenmodes,

$$r_1 = \frac{i\zeta(1+\cos^2\theta)/2}{\cos\theta - i\frac{\zeta}{2}(\cos^2\theta+1)} , \quad r_2 = 0 . \tag{A10}$$

For normal incidence ($\theta=0$) the eigenpolarizations are positive and negative circular polarizations, with reflection and transmission coefficients for σ^+ reducing to Eq. (3a). Furthermore, it is clear from Eq. (A10) that for small angles the reflection coefficient deviates from the normal incident case only to order θ^2, thus imposing no stringent requirements on beam collimation.

[1] P. Verkerk *et al.*, Phys. Rev. Lett. **68**, 3961 (1992).

[2] P. S. Jessen *et al.*, Phys. Rev. Lett. **69**, 49 (1992).

[3] A. Hemmerich and T. W. Hänsch, Phys. Rev. Lett. **70**, 1410 (1993).

[4] G. Grynberg *et al.*, Phys. Rev. Lett. **70**, 2249 (1993).

[5] A. Hemmerich, C. Zimmermann, and T. W. Hänsch, Europhys. Lett. **22**, 89 (1993).

[6] P. Verkerk *et al.*, Europhys. Lett. **26**, 171 (1994).

[7] L. Brillouin, *Wave Propagation in Periodic Structures,* 2nd ed. (Dover, New York, 1946); P. Yeh and A. Yariv, *Optical Waves in Layered Media* (Wiley, New York, 1988).

[8] See J. Opt. Soc. Am. B **10** (2) (1993), special issue on photonic band gaps; J. Mod. Opt. **41**, (2) (1994), special issue on photonic band gaps, edited by G. Kurizki and J. W. Haus.

[9] B. Lounis *et al.*, Europhys. Lett. **21**, 13 (1993); A. Hemmerich, M. Weidemüller, and T. Hänsch, *ibid.* **27**, 42 (1994).

[10] (a) C. Cohen-Tannoudji and F. Laloë, J. Phys. (Paris) **28**, 505 (1967); **28**, 722 (1967); (b) A. V. Bezverbnyi, V. S. Smirnov, and A. M. Tumaikin, Zh. Eksp. Teor. Fiz. **105**, 62 (1994) [Sov. Phys. JETP **78**, 33 (1994)].

[11] M. Born and E. Wolf, *Principles of Optics,* 6th ed. (Pergamon, Oxford, 1989), pp. 99 and 634.

[12] Although the mean force of an atom at the node of a standing wave is zero, there is always a nonvanishing fluctuation in the dipole force. See C. Cohen-Tannoudji, in *Atomic Motion in Laser Light, 1990 Les Houches Lectures,* Session LIII, edited by J. Dalibard, J. M. Raimond, and J. Zinn-Justin (Elsevier Science, Amsterdam, 1992), pp. 59–78.

[13] See, for example, M. V. Klein and T. E. Furtak, *Optics,* 2nd ed. (Wiley, New York, 1986), pp. 295–300.

[14] N. W. Ashcroft and N. D. Mermin, *Solid State Physics* (Holt-Saunders, Philadelphia, 1976), pp. 146–148.

[15] J. Dalibard and C. Cohen-Tannoudji, J. Opt. Soc. Am. B **6**, 2023 (1989); P. J. Ungar, D. S. Weiss, E. Riis, and Steven Chu, J. Opt. Soc. Am. B **6**, 2058 (1989).

[16] In general the detuning of the lattice lasers will affect the temperature of the atoms and thus their localization. We assume that all detunings are chosen so that the atoms are sufficiently cooled that our approximations are valid.

[17] W. Happer, Rev. Mod. Phys. **44**, 169 (1972).

[18] U. Eichmann, in *Laser Spectroscopy,* edited by Louis Bloomfield, Thomas Gallagher, and Daniel Larson, AIP Conf. Proc. No. 290 (AIP, New York, 1993), pp. 43–48.